# Stator interturn short circuit fault identification in DFIG and its analysis using an artificial neural network

**Vivek Kushwaha[1,2], Sanjay Kumar Maurya[3], Arvind Kumar Yadav[1]**
[1]Department of Electrical Engineering, Institute of Engineering and Technology, GLA University, Uttar Pradesh, India
[2]Department of Electrical Engineering, Gyan Ganga Institute of Technology and Sciences (GGITS), Madhya Pradesh, India
[3]Department of Electrical Engineering, Samrat Ashok Rajkiya Engineering College, Mirzapur, India

**Article Info**

***Article history:***

Received May 7, 2026
Revised Jul 30, 2026
Accepted Aug 24, 2026

***Keywords:***

Artificial neural network
Doubly-fed induction generator
Inter-turn short circuit fault
Simulation
Stator current

**ABSTRACT**

Inter-turn short circuit (ITSC) issues are a common electrical failure mainly caused by the deterioration of winding insulation in the machine over time. Failing to detect such issues early can lead to catastrophic consequences. This article investigates the interturn fault in the stator winding of a doubly-fed induction generator (DFIG) used in wind turbines. A flux linkage difference vector (FLDV) model is introduced in this study for fault detection. Additionally, an artificial neural network (ANN) model is proposed to classify these faults. Specifically, a short-circuit fault is induced in each phase of the stator winding, and the faults are classified by assigning different magnitudes to the respective phases. The ANN is trained to identify which phase contains an interturn fault, with output waveform amplitudes of 1, 2, or 3 corresponding to faults in phases "a," "b," and "c." If no fault is present, the waveform magnitude is designated as "0." This approach enables early fault diagnosis by analyzing waveform patterns, thereby preventing overheating caused by short circuits and avoiding severe, irreversible damage to the windings.



***Corresponding Author:***

Vivek Kushwaha
Department of Electrical Engineering, Institute of Engineering and Technology, GLA University
Mathura 281406, Uttar Pradesh, India
Email: vivekkushwaha@ggits.org, vvv2427980@gmail.com

## 1. INTRODUCTION

The escalating global energy demand and rising environmental worries have hastened the shift to renewable energy sources. Among these, wind and solar energy have emerged as the most widely adopted options because of their sustainability and availability. Wind energy conversion systems (WECS) are crucial for contemporary electricity generation, with doubly fed induction generators (DFIGs) being widely utilized because of their high efficiency, ability to operate at variable speeds, and independent management of active and reactive power. Even with these benefits, DFIGs are susceptible to different types of electrical faults, with inter-turn short circuit (ITSC) faults in stator windings being especially serious. ITSC faults lead to a rise in localized current, overheating, deterioration of insulation, and ultimately machine failure if they are not caught early on. Hence, to guarantee dependable functioning, lower upkeep expenses, and avert power loss, it is crucial to detect ITSC faults accurately and promptly.

Due to the growing use of wind energy and the requirement for dependable operation, fault detection and condition monitoring of DFIG-based wind energy conversion systems have drawn a lot of research interest. Numerous studies have used various signal processing and intelligent diagnostic techniques to examine electrical, mechanical, sensor, and converter faults in DFIG system. Atteyeh *et al.* [1] created a thorough dq-axis MATLAB/Simulink model of a 2 MW DFIG for faulty and healthy operation conditions.

The study showed that electromagnetic torque, dq-axis voltages, and stator currents are particularly sensitive to winding and bearing problems, making them helpful indicators for condition monitoring. In a similar vein, a stator current amplitude ratio-based method for diagnosing drivetrain faults was put out in [2], and its efficacy was confirmed through experimental testing under a range of operating circumstances. One of the most serious electrical problems in DFIGs is rotor winding issues. A Symmetric Impedance Deviation (SID)-based diagnostic method was introduced in [3] to differentiate between rotor inter-turn and inter-phase short circuits. Using symmetrical component analysis of rotor currents, the technique correctly determined the kind and severity of the problem. Additionally, in order to enhance fault tolerance against current sensor failures while preserving acceptable dynamic performance, a different stator current-based backstepping control technique was put out in [4]. In [5], a machine learning-based method for identifying faults via negative-sequence current analysis was presented. Under various operating conditions, the identification accuracy was 98%. Similarly, a hybrid intelligent framework with a 99% localization accuracy was created in [6] for stator current sensor problem diagnostics by using the unscented Kalman filter (UKF) in addition to an artificial neural network (ANN).

The literature has put forth several methods for identifying and diagnosing ITSC defects in DFIGs. A zero-sequence voltage-based method is introduced, using MATLAB-based modelling and simulation to facilitate fault detection and localization [7]. A 100 kW DFIG wind turbine's issue is diagnosed via correlation analysis between vibration signals and external magnetic signals in [8]. Stator and rotor flaws are examined under controlled conditions utilizing a 5-kW test setup for experimental validation. There has also been much research done on advanced signal processing methods [9]. The notion of magnetic flux leakage (MFL) is used to identify early defects [10]. Stator interturn defects are identified and their severity assessed using motor current signature analysis (MCSA) in conjunction with multi-scale Park's vector approach [11]. For automated DFIG testing, the inverted embedded offline test is used in [12]. The suggested technique detects and categorizes the defects in the stator core interlaminar insulation, rotor winding turn insulation, and slip ring brush contact. A micromachine and a standard small store-bought wound rotor induction machine (WRIM) are compared in [13]. In this study, rotor interturn faults in large-scale and micromachines are compared. Because micromachines are proportionate replicas of bigger machines, they offer an ideal representation of what is expected under the transient operating conditions of wind turbines. This would facilitate the development of condition monitoring solutions suitable for the industry's real systems. [14] suggests the enlarged Park's vector method, which calculates the mathematical relationship between unbalanced voltage, load variation, and the negative sequence current in the stator using the Fryze-Buchholz-Dpenbrock algorithm and the non-linear least squares approach.

A model based on the finite element method (FEM) is developed in [15] to comprehend the machine's behavior in both healthy and ITSC fault conditions in the rotor winding. The study [16] proposes deep learning-based convolutional neural networks (CNNs) with non-intrusive infrared imaging for precise defect localization and classification. In ITSC fault detection, model-based and observer-based approaches have demonstrated encouraging outcomes. A new fault feature for precise diagnosis is offered by the bilateral flux linkage difference vector (FLDV) approach, which was first presented in [17]. In [18], models based on the Finite Element Method (FEM) are created to examine machine behaviour in both faulty and healthy scenarios. For DFIG wind turbines, a fault ride-through technique is suggested in [19] for stator interturn short-circuit faults. The suggested concept reduces maintenance when an ITSC failure occurs, increases operating capacity, and prevents power loss from shutdown. A robust method for estimating rotor ITSC defects is devised using an H-infinity observer [20].

An experimental system is created to mimic the real operation of a wound rotor induction machine (WRIM) [21]. The stator ITSCF is detected using empirical mode decomposition (EMD) and time-domain analysis. Additionally, compared to traditional procedures, data-driven approaches like long short-term memory (LSTM) networks in [22] show better diagnostic accuracy and quicker reaction. For fault identification, statistical analysis and frequency-domain techniques are also frequently employed. An experimental setup has been constructed in [23] to identify the ITF in the rotor turns of a DFIG with a magnetic flux measuring coil antenna. It suggests that, to identify an ITSC problem in a DFIG, search coil voltage at various frequencies is a more efficient and sophisticated method than current signature analysis. Fault-related features can be effectively extracted using methods like power spectral density (PSD), time synchronous averaging (TSA) [24], Kalman filtering [25], maximum power point tracking (MPPT)-based detection [26], and TSA; CSA techniques are applied in [27] to detect faults. An ITSC fault between the rotor and stator is hypothesized. Here, the best active power production for varying wind speeds is ensured by applying maximum power point tracking (MPPT) management [28].

Winding function analysis (WFA), dq0 transformation, and multi-circuit theory are examples of advanced modelling techniques that have been used to enhance fault analysis and comprehension [29]. Additionally, measures including RMS current, total harmonic distortion (THD), sequence components, and phase differences are used in analytical and experimental research to detect ITSC faults [30]-[32]. The fast Fourier transform is suggested in [33], and multi-circuit theory is suggested in [34], and the outcomes of the suggested experimental model are confirmed for ITSC fault detection. Inter-turn short circuit (ITSC) fault detection in doubly fed induction generator (DFIG)-based wind energy systems has been extensively studied, but there are still a few important issues that need to be addressed. For example, many of the current methods rely on intrusive measurement techniques, expensive sensors, or complex mathematical modelling, which restricts their practical implementation in real-time applications. Signal processing approaches like FFT, CNN, SVM, and MCSA frequently fail to detect incipient faults under varying load and noise conditions, and they are costly too, while model-based and observer-based techniques are sensitive to parameter variations and modelling errors. Moreover, even while data-driven methods like deep learning have demonstrated encouraging outcomes, they frequently need big datasets, a lot of processing power, and are difficult to understand. As a result, a reliable, precise, and computationally effective technique for early-stage ITSC fault detection under various operating situations is required.

The integrated phase-wise stator ITSC identification framework for a DFIG wind turbine is what makes this work innovative, even though FLDV-based detection and ANN-based fault classification have been documented in earlier works. The proposed framework integrates supervised machine-learning classification with the variations in FLD and FLDV caused by stator-winding impedance imbalance. The classifier output is encoded into four operational classes: phase-a stator ITSC, phase-b stator ITSC, phase-c stator ITSC, and healthy state. Therefore, instead of just determining whether an abnormal state exists, the method performs phase localization of the stator ITSC defect. This work's primary contributions are listed as follows: i) Firstly, a wind-turbine model for healthy and phase-wise stator ITSC conditions is created using MATLAB/Simulink DFIG. To determine how shorted stator turns affect current, voltage, and flux-linkage behavior, the FLD and FLDV responses are examined; ii) Then, phase ‘a’, phase ‘b’, and phase ‘c’ ITSC faults and healthy operation are represented by four output classes in a trained diagnostic dataset; iii) Thereafter, an ANN classifier is created for automatic fault identification, and an SVM classifier is incorporated as a comparative baseline; and iv) Finally, classification metrics and confusion matrices are used to assess the diagnostic performance, allowing for a clear interpretation of the model accuracy and phase-wise classification behavior.

## 2. DFIG SIMULATION MODEL

Figure 1 displays the entire MATLAB/Simulink-based DFIG wind-turbine model utilized in this investigation. The simulated generator has a rating of 400 V, 50 Hz, and 1 MVA. There are 48 and 32 turns in the stator and rotor windings, respectively. The rotor winding is regarded as healthy, and the inquiry is restricted to stator interturn short-circuit defects. To investigate the phase-wise response of the DFIG, a five-turn short circuit is introduced independently in the stator phases. Phase A faults occur between 0.5 and 0.7 seconds, Phase B faults occur between 1.1 and 1.4 seconds, and Phase C faults occur between 1.5 and 1.7 seconds. The healthy operational condition is represented by the remaining time periods. Three-phase stator current, three-phase stator voltage, active power, reactive power, flux linkage difference (FLD), flux linkage difference vector (FLDV), and the classifier output are among the logged signals. The target classes are represented by the following codes: 0 for healthy operation, 1 for phase-a ITSC, 2 for phase-b ITSC, and 3 for phase-c ITSC. The suggested method can detect both the impacted phase and the existence of a stator ITSC fault.

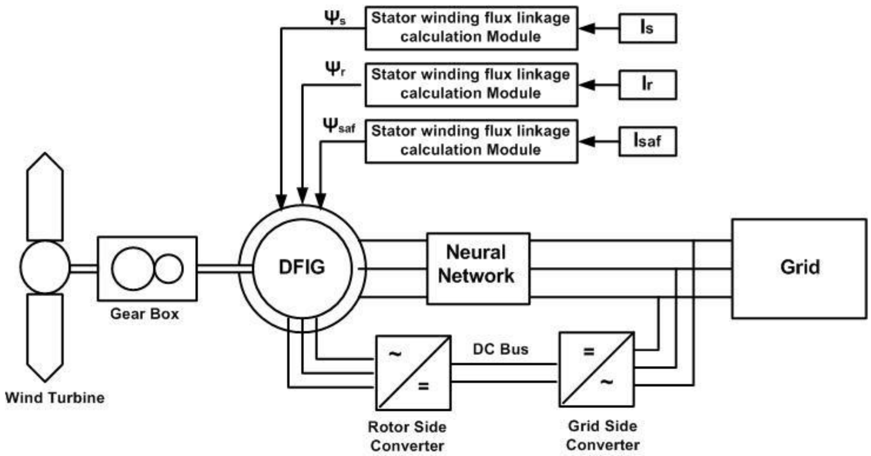


Figure 1. Schematic diagram of simulation model

## 3. INTERTURN SHORT CIRCUIT FAULT

An ITSC defect is characterized by the short-circuiting of 2 or more turns in the stator or rotor winding. Because of this fault, the current suddenly increases in the phase where the fault occurred, which increases the temperature in the winding. Due to the continuous heating in the winding for a long time, it may damage the whole winding. Therefore, to save the machine from severe damage, it is required to diagnose the fault at an early stage and take necessary action. The neural network tool in MATLAB/Simulink is applied to diagnose the interturn fault in the stator winding.

### 3.1. Mathematical modelling of ITF

In this study, faults are introduced in all three phases for different durations. As shown in Figure 2, an inter-turn fault in phase ‘a’ is created by short-circuiting the phase winding. Similarly, an inter-turn fault can be introduced in each phase. The number of turns in the stator winding is given by $N_s$ = 48, and the number of turns in the rotor winding is $N_r$ = 32. The turns ratio is given by $a = \frac{N_s}{N_r} = \frac{48}{32} = 1.5$. The number of short-circuited turns in the stator winding is denoted by $N_{sf}$. The number of healthy turns remaining in the stator winding is given by $N_{srm} = N_s - N_{sf}$. The magnetic permeance is denoted by $\mathcal{P}$. The inductance of the short-circuited turns is expressed as $L_{sf} = N_s^2\mathcal{P} = L_s\left(\frac{N_{sf}}{N_s}\right)^2$. The inductance of the remaining healthy turns is expressed as $L_{srm} = (N_s - N_{sf})^2\mathcal{P} = L_s\left(\frac{N_s-N_{sf}}{N_s}\right)^2$. The mutual inductance between the short-circuited turns and the remaining healthy turns in the same phase is given by $M_{sfrm} = N_{sf}(N_s - N_{sf})\,\mathcal{P} = L_s\,\frac{N_{sf}(N_s-N_{sf})}{N_s^2}$. Therefore, the per-phase inductance matrix is given by $L_{sfrm} = \begin{bmatrix} L_{sf} & M_{sfrm} \\ M_{sfrm} & Ls_{rm} \end{bmatrix}$. The resistance per turn is given by $R_{pt} = \frac{R_s}{N_s}$.

The resistance of short-circuited turns is expressed as (1).

$$R_{sf} = N_{sf} \cdot R_{pt} = R_s\,\frac{N_{sf}}{N_s} \tag{1}$$

Resistance of the remaining healthy turns:

$$R_{srm} = \left(N_s - N_{sf}\right) R_{pt} = R_s\,\frac{N_s-N_{sf}}{N_s} \tag{2}$$

$$\begin{bmatrix} \psi\Phi_s \\ \psi_r \\ \psi_{sf} \end{bmatrix} = \begin{bmatrix} L_{ss} & M_{sr} & L_{sfrm} \\ M_{sr} & L_{rr} & 0 \\ L_{sfrm} & 0 & L_{sf} \end{bmatrix} \begin{bmatrix} I_s \\ I_r \\ I_{sf} \end{bmatrix} \tag{3}$$

$$\begin{bmatrix} V_s \\ V_r \\ V_{sf} \end{bmatrix} = \begin{bmatrix} R_{ss} & 0 & 0 \\ 0 & R_{rr} & 0 \\ 0 & 0 & R_{sf} \end{bmatrix} \begin{bmatrix} I_s \\ I_r \\ I_{sf} \end{bmatrix} + \mathcal{P} \begin{bmatrix} \psi_s \\ \psi_r \\ \psi_{sf} \end{bmatrix} \tag{4}$$

V, I, and ψ The voltage, current, and flux linkage matrices are shown in (3) and (4). Where the subscripts s, r, and f represent stator, rotor, and fault, respectively. L, R, and M represent the self-inductance, resistance, and Mutual inductance.

$$L_{ss} = \begin{bmatrix} \mu^2(L_{ls} - L_{ms}) & -\frac{\mu}{2}L_{ms} & -\frac{\mu}{2}L_{ms} \\ -\frac{\mu}{2}L_{ms} & (L_{ls} - L_{ms}) & -\frac{\mu}{2}L_{ms} \\ -\frac{\mu}{2}L_{ms} & -\frac{\mu}{2}L_{ms} & (L_{ls} - L_{ms}) \end{bmatrix} \tag{5}$$

$$L_{rr} = \begin{bmatrix} \zeta^2(L_{lr} - L_{mr}) & -\frac{\zeta}{2}L_{mr} & -\frac{\zeta}{2}L_{mr} \\ -\frac{\zeta}{2}L_{mr} & (L_{lr} - L_{mr}) & -\frac{\zeta}{2}L_{mr} \\ -\frac{\zeta}{2}L_{mr} & -\frac{\zeta}{2}L_{mr} & (L_{lr} - L_{mr}) \end{bmatrix} \tag{6}$$

$L_{ss}$ and $L_{rr}$ are the self-inductance matrices of the stator and rotor windings, respectively. Here μ and ζ are the short-circuit coefficients for the stator and rotor windings, respectively. The short-circuit coefficient for the stator winding is defined as μ = no. of fault turns in stator winding/total no. stator winding and ζ = no. of fault turns in the rotor winding/total no. rotor winding. If there is no fault, then the value of the short-circuit coefficient will be ‘0’.

$$M_{sr} = L_{sr}\begin{bmatrix} \mu\zeta cos\Theta & \mu\cos(\Theta+120^0) & \mu\cos(\Theta-120^0) \\ \zeta\cos(\Theta-120^0) & cos\Theta & \cos(\Theta+120^0) \\ \zeta\cos(\Theta+120^0) & \cos(\Theta-120^0) & cos\Theta \end{bmatrix} \tag{7}$$

Where $M_{sr}$ is the mutual inductance matrix between stator and rotor.

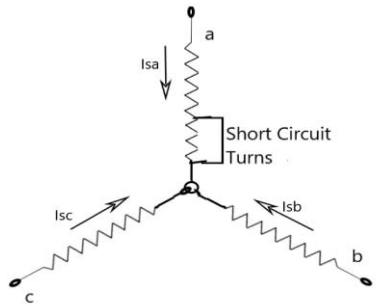


Figure 2. Short-circuit diagram of stator winding

### 3.2. Identification method based on FLDV

Flux linkages in a DFIG can be shown as in the following equation. The (8) and (9) represent the current and voltage models to get the flux linkages for the DFIG.

$$[\Psi_i] = \begin{bmatrix}\psi_{si}\\ \psi_{ri}\end{bmatrix} = \begin{bmatrix}L_{ss} & M_{sr}\\ M_{sr} & L_{rr}\end{bmatrix}\begin{bmatrix}I_s\\ I_r\end{bmatrix} \tag{8}$$

$$\mathcal{P}[\psi_v] = \mathcal{P}\begin{bmatrix}\psi_{sv}\\ \psi_{rv}\end{bmatrix} = \begin{bmatrix}V_s\\ V_r\end{bmatrix} - \begin{bmatrix}R_{ss} & 0\\ 0 & R_{rr}\end{bmatrix}\begin{bmatrix}I_s\\ I_r\end{bmatrix} \tag{9}$$

The DFIG is affected by the slip ratio; the rotor current fault features are diminished, and it is challenging to precisely identify the rotor-side ITF, which are limitations of the existing diagnosis approach as a characteristic quantity. Therefore, a new approach is proposed, characterized by the flux linkage and the flux linkage difference vector (FLDV). Due to the fluctuation in the impedance of the stator and rotor windings before and after the ITF, the observed fault voltage and current are incorporated into the voltage and flux equations. Thus, the flux linkage obtained is:

$$\Delta\psi = \psi_i - \psi_v \tag{10}$$

$$\boldsymbol{\Delta}\psi = \begin{bmatrix}L_{ss} & M_{sr}\\ M_{sr} & L_{rr}\end{bmatrix}\begin{bmatrix}I_s\\ I_r\end{bmatrix} - \int\left(\begin{bmatrix}V_s\\ V_r\end{bmatrix} - \begin{bmatrix}R_{ss} & 0\\ 0 & R_{rr}\end{bmatrix}\begin{bmatrix}I_s\\ I_r\end{bmatrix}\right) \tag{11}$$

The (10) and (11) represent a fault characteristic quantity. $\Psi_i$and $\psi_v$ are current and voltage models, respectively, and their difference represents the flux linkage difference (FLD).

$$£_s = \Delta\psi_{sa} + \Delta\psi_{sb} + \Delta\psi_{sc} \tag{12}$$

$$£_r = \Delta\psi_{ra} + \Delta\psi_{rb} + \Delta\psi_{rc} \tag{13}$$

$£_s$ and $£_r$ are the respective FLDVs in the stator and rotor windings. The stator and rotor FLDVs rotate at different frequencies because of the DFIG's asynchronous motor features. The slip ratio is multiplied by the rotor FLDV frequency, while the FLDV frequency of the stator is the power frequency. It is possible to determine whether an ITF happens on the rotor or the stator using this frequency.

### 3.3. FLDV theory

Assume that the phase ‘a’ of the stator winding is short-circuited and it short-circuit factor is ‘μ’. The FLDV calculation formula under fault conditions is represented by (11). Now,

$$\varDelta\psi_s = \begin{bmatrix}\varDelta\psi_a\\ \varDelta\psi_b\\ \varDelta\psi_c\end{bmatrix} = \psi_{si} - \psi_{sv} = [L_{ss}\ \ M_{sr}]\begin{bmatrix}I_{sf}\\ I_{rf}\end{bmatrix} - \int\left(V_{sf} - [R_{ss}\ \ 0]\begin{bmatrix}I_{sf}\\ I_{rf}\end{bmatrix}\right) \tag{14}$$

Suffix f indicates faulty quantities with DFIG parameters in (14). Calculation of the short-circuit additional flux linkage in the fault model is not required, as there is no additional term for the fault in the normal machine model. The values of flux linkage obtained from the voltage and flux linkage equations by a typical DFIG are the same.

$$\varDelta\psi_s = \varDelta\psi_{si} - \varDelta\psi_{sv} = (\psi_{sif} - \psi_{sih}) - (\psi_{svf} - \psi_{svh}) \tag{15}$$

In (15), the faulty and healthy DFIGs' current equations represent the changes to the flux difference. This allows FLDV to be calculated separately.

$$\begin{aligned}\varDelta\psi_{sia} &= (\psi_{siaf} - \psi_{siah})\\ \varDelta\psi_{sia} &= (L_{ls} - L_{ms})(\mu^2 - 2\mu)\, I_{sa} + \mu(1-\mu)L_{ms}L_f + \frac{\mu}{2}L_{ms}(I_{sb} + I_{sc}) -\\ &\quad \mu L_{sr}[I_{ra}cos\Theta + I_{rb}\cos(\Theta + 120^0) + I_{rc}\cos(\Theta - 120^0)]\end{aligned} \tag{16}$$

The 3-phase unbalanced rotor current can be neglected for the stator phase 'a' term ITF; therefore, the last term in (15) can be ignored.

$$\varDelta\psi_{sia} = (L_{ls} - L_{ms})(\mu^2 - 2\mu)\, I_{sa} + \mu(1-\mu)L_{ms}L_f + \tfrac{\mu}{2}L_{ms}(I_{sb} + I_{sc}) \tag{17}$$

Similarly, the flux linkage of the healthy phase of stator winding 'b' & 'c' is given by (18).

$$\varDelta\psi_{sib} = \varDelta\psi_{sic} = \tfrac{\mu}{2}L_{ms}\left(I_{sa} + I_{saf}\right) \tag{18}$$

$$\varDelta\psi_{ri} = \begin{bmatrix}\varDelta\psi_{ia}\\ \varDelta\psi_{ib}\\ \varDelta\psi_{ic}\end{bmatrix} = \mu L_{sr}\left(I_{saf} - I_{sa}\right)\begin{bmatrix}cos\Theta\\ cos(\Theta + 120^0)\\ cos(\Theta - 120^0)\end{bmatrix} \tag{19}$$

The flux linkage of the healthy winding of each phase in the rotor is shown in (19). The FLD in the voltage equation is obtained from (20) and (21).

$$\mathcal{P}\varDelta\psi_{sva} = \mathcal{P}\psi_{svaf} - \mathcal{P}\psi_{sva} = \mu R_s\left(I_{saf} - I_{sa}\right) \tag{20}$$

Assume $I_{saf} - I_{sa} = Asin(\omega + \Theta_0)$:

$$\varDelta\psi_{sva} = -\tfrac{\mu R_s A}{\omega}\cos(\omega t + \Theta_0) \tag{21}$$

By using (17)-(21), six-phase FLDs can be found. Also, (11) & (12) give FLDV. From (20) and (21), FLDs of the 3-phase rotor winding are symmetrical, so their sum ($£_r$) is zero. Concerning the stator windings, the amplitude of fault phase 'a' differs significantly from that of the other phases. Since the vector sum of $I_{sb}$ and $I_{sc}$ is directed opposite to that of $I_{sa}$, $I_{saf}$ follows the same direction as $I_{sa}$. Phase 'a' FLD angle tracks its current. In the case of an ITF in the stator, the fault current typically exhibits a higher amplitude than that of the stator current. Consequently, the FLD in the other two phases will be opposite to that of phase 'a'. Now, FLDV of the stator winding is obtained as (22) and (23).

$$\begin{aligned}£_s = {}& \mu L_{ls}(\mu - 2)I_{sa} + \tfrac{\mu R_s A}{\omega}cos(\omega t + \Theta_0) + \mu L_{ms}\Big[\left(\mu - \tfrac{5}{2}\right)I_{sa} + \left(\tfrac{3}{2} - \mu\right)I_{saf} +\\ & \tfrac{1}{2}\left(I_{sb} + I_{sc}\right)\Big]\end{aligned} \tag{22}$$

$$\begin{aligned}£_r = {}& \mu L_{lr}(\mu - 2)I_{ra} + \tfrac{\mu R_r A}{\omega}cos(\omega t + \Theta_0) + \mu L_{mr}\Big[\left(\mu - \tfrac{5}{2}\right)I_{sa} + \left(\tfrac{3}{2} - \mu\right)I_{saf} +\\ & \tfrac{1}{2}\left(I_{sb} + I_{sc}\right)\Big]\end{aligned} \tag{23}$$

## 4. ARTIFICIAL NEURAL NETWORK (ANN)

An ANN is based on the composition and capabilities of the human brain, analyzes data, and draws conclusions by using interconnected nodes, or artificial neurons. Neural networks are helpful for image identification, natural language processing, and predictive analytics applications because of their capacity to learn from data and spot patterns. Training data is essential for neural networks to learn and gradually increase their accuracy. A standard feed-forward ANN, often called a Multilayer Perceptron (MLP), is composed of an input layer, one or more hidden layers, and an output layer, as shown in Figure 3.

Each layer consists of interconnected nodes (neurons) that process information using non-linear activation functions, enabling the network to learn complex patterns from data. The learning process is governed by a training algorithm, with backpropagation being the most fundamental method. Backpropagation calculates the gradient of a loss function (cross-entropy) with respect to the network's weights, allowing the model to iteratively adjust its parameters via an optimization algorithm like Stochastic Gradient Descent (SGD) or Adam to minimize prediction error. This capability to learn intricate, non-linear decision boundaries without explicit feature engineering makes ANNs highly effective for classification tasks such as the fault diagnosis presented in this work.

The outcome of the simulation was transformed into a dataset for supervised classification. Depending on the applicable operating condition, a class label was given to each sample. Phase-a ITSC was designated as 1, phase-b ITSC as 2, phase-c ITSC as 3, and the healthy state as 0. Phase A fault windows were 0.5-0.7 s, phase B was 1.1-1.4 s, and phase C was 1.5-1.7 s. Samples that are extremely near to the beginning and end of each fault period may be omitted from training or handled carefully during performance evaluation in order to prevent ambiguity at switching instants.

Quantities that physically react to stator interturn short-circuit failures were used to choose the diagnostic inputs. These comprise active power, reactive power, FLD, FLDV, three-phase stator currents, and three-phase stator voltages. Because an ITSC fault lowers the faulty phase's effective impedance, the accompanying voltage and flux-linkage behavior change, and the current magnitude in that phase increases. Thus, each analysis window was used to extract time-domain features, including mean value, root-mean-square value, standard deviation, maximum value, minimum value, peak-to-peak value, energy, skewness, kurtosis, and phase-current/phase-voltage imbalance ratios. The SVM and ANN classifiers received these features as inputs.

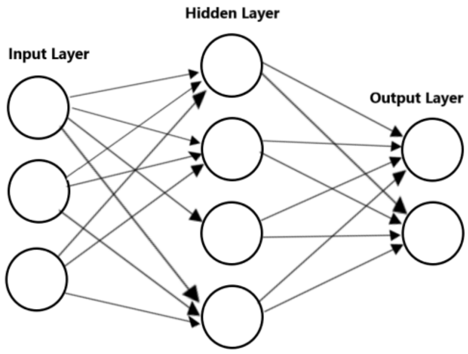


Figure 3. Neural network model

## 5. RESULTS AND DISCUSSION

The simulation results obtained using MATLAB/Simulink are shown in Figures 4 and 5. The simulation model shown in Figure 1 consists of a 1 MVA, 400 V, 50 Hz DFIG wind turbine connected to a neural network model. In the proposed model, ITFs are introduced simultaneously in phases 'a', 'b', and 'c'. Figure 4 presents the waveforms of the healthy DFIG, including the per-unit values of the three-phase voltage, current, active power, and reactive power in Figures 4(a)–4(d), respectively. The waveforms of each quantity, namely voltage, current, active power, and reactive power, exhibit normal characteristics without disturbances, indicating the healthy operating condition of the machine.

Next, the inter-turn fault is considered in the stator winding only, while the rotor winding remains healthy. Different results are obtained, as shown in Figures 5(a)–5(h) (see Appendix). First, 5 turns in phase 'a' of the stator winding are short-circuited from 0.5 to 0.7 s. As shown in Figure 5(a), the FLD is '0' before 0.5 s because the machine is operating under healthy conditions. When the fault occurs, the magnitude of the FLD increases. Similarly, the magnitude of the FLDV increases, as shown in Figure 5(b). Thus, the current signature of phase 'a' of the stator winding shows an increase in magnitude, as shown in Figure 5(c), between

0.5 and 0.7 s, while the corresponding voltage response is shown in Figure 5(d). The magnitude of the current in phase ‘a’ increases, as indicated by the red waveform in Figure 5(c), because the impedance of that phase is reduced. At the same time, the amplitude of the voltage in phase ‘a’ decreases, as indicated by the red waveform in Figure 5(d).

Similarly, the fault is created in phase ‘b’. Figures 5(e) and 5(f) represent the ITF involving 5 turns in phase ‘b’ of the stator winding from 1.0 to 1.3 s. Figure 5(e) shows an increased amplitude of the current in phase ‘b’, represented by the yellow waveform, while the amplitude of the voltage in phase ‘b’ decreases at the same time, as shown by the yellow waveform in Figure 5(f). Next, the ITF is established in phase ‘c’ of the stator winding, as shown in Figures 5(g) and 5(h), from 1.5 to 1.7 s. Here, the amplitude of the current in phase ‘c’ also increases, as shown by the blue waveform in Figure 5(g), while the voltage response in Figure 5(h) shows that the peaks of the blue waveform are shorter than those of the other phase voltages.

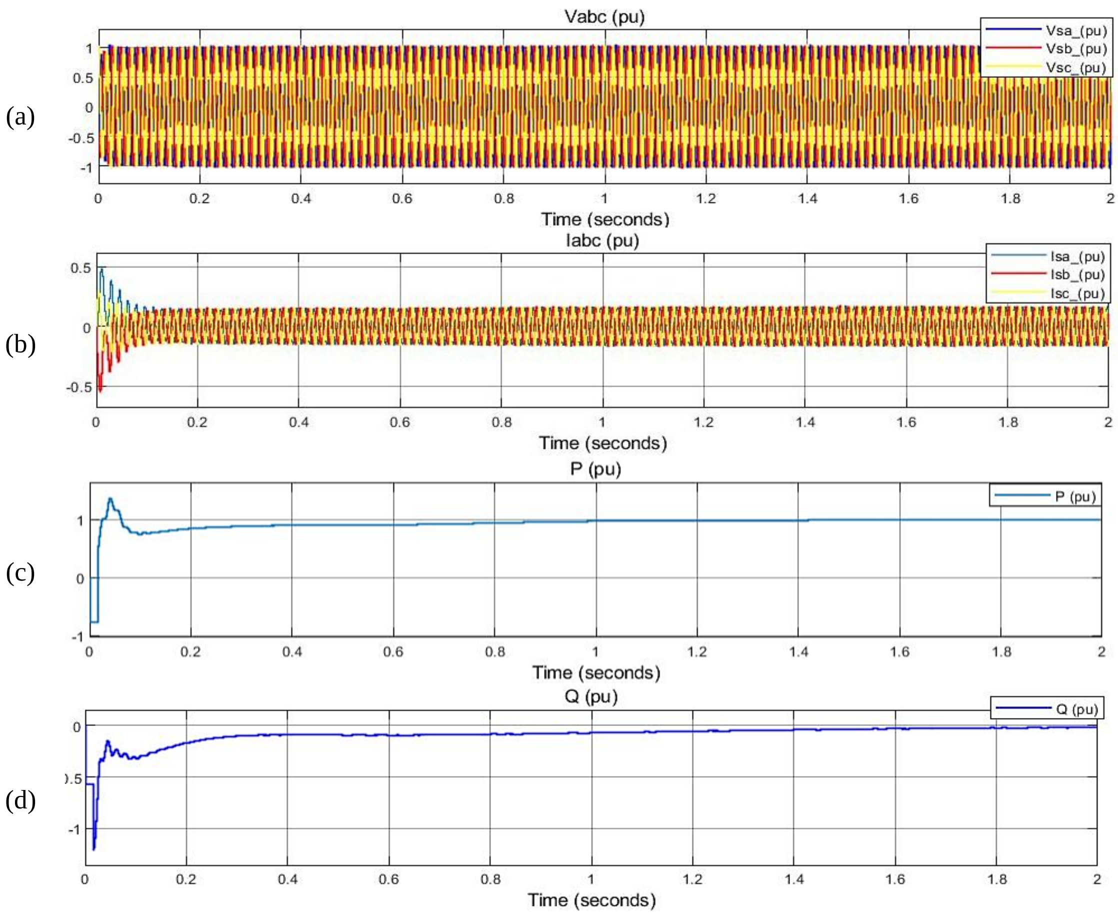


Figure 4. The waveform of (a) 3-phase voltage, (b) current, (c) active, and (d) reactive power for DFIG under normal conditions

As the current increases in the winding, the temperature of the winding also increases, which may cause insulation failure and therefore increase the risk of permanent damage to the winding. Therefore, it is necessary to identify the inter-turn fault at an early stage to protect the machine from damage and obtain stable and reliable power in the system. Thus, the neural network tool is applied in MATLAB for fault classification and identification. First, the model is trained for faults occurring in all phases at different times, and each phase is assigned a different magnitude. After that, the trained neural network model is connected to the DFIG simulation model, which further identifies the fault in the windings according to the training.

In MATLAB's Neural Network Toolbox, the "best" performance range for a regression curve depends on the specific problem and data, but generally, a low mean squared error (MSE) and a high R-value (correlation coefficient) indicate good performance. The range of performance for a regression curve depends on the problem and data, but a low value of MSE, i.e., close to ‘0’, and a high R-value (correlation coefficient), i.e., close to 1, indicate good performance. A high R-value means that the predicted and actual values are strongly correlated along a straight line, which indicates that the regression is accurate. Figure 6 indicates that the best validation performance is 0.10393 at epoch 23 (i.e., 23 iterations), which means that the value of MSE is close to ‘0’, i.e., 0.10393. Thus, the training performance curve indicates good performance of the neural network. Figure 7 shows the regression curve of the neural network for training, validation, and testing. For training, the value of R = 0.96967; for validation, R = 0.95374; and for testing, R = 0.96957, with an overall R-value of 0.96715. Therefore, the regression curve also indicates good performance, as the R-value is very close to 1.


Figure 6. Training performance curve of neural network by MATLAB

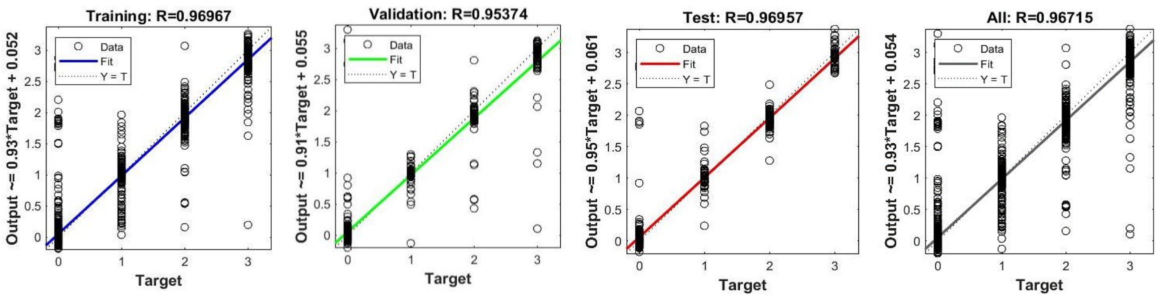


Figure 7. Regression curve of neural network by MATLAB for training, validation, and test

Here, a feed-forward artificial neural network (ANN) is developed for the multi-class classification of the operational state of a system into one of four categories: Healthy, phase ‘a’ fault, phase ‘b’ fault, and phase ‘c’ fault. Figure 8 shows the confusion matrix for the total dataset, which comprises 10,001 samples, with a notable class imbalance. The Healthy class contains 1,301 instances, while the phase ‘a’ and phase ‘c’ fault classes each contain 200 instances, and the phase ‘b’ fault class contains 300 instances. To mitigate the bias introduced by this imbalance, the synthetic minority over-sampling technique (SMOTE) was applied to the training partition to generate synthetic samples for the minority classes.

The model architecture consisted of an input layer, two hidden layers with 64 and 32 neurons, respectively, employing the rectified linear unit (ReLU) activation function, and an output layer with four neurons using the Softmax function to output class probabilities. The model was compiled with the Adam optimizer and categorical cross-entropy loss function and was trained for 100 epochs with a batch size of 32. The model’s performance was evaluated on a hold-out test set. The resulting confusion matrix demonstrated exceptional classification capability, with the model correctly classifying 1296 out of 1301 Healthy instances, 199 out of 200 instances for phase ‘a’ & ‘c’ fault, and 299 out of 300 instances for phase ‘b’ fault, achieving a final overall classification accuracy of 99.60%.

Previously, authors [17], [18], [21] analyzed the ITSC fault (like 2 or 5 turns shorted) for a particular phase of the stator winding. But, in this study, the faults are created in all the 3 phases; they are classified by different amplitudes. As per training the Figure 9 shows, that fault in phase ‘a’ which is occurred between time 0.5 sec to 0.7 sec having amplitude 1, further fault occurred in phase ‘b’ is in between time 1.1 sec to 1.4 sec having amplitude 2 and fault occurred in phase ‘c’ is in between time 1.5 to 1.7 sec having amplitude 3. This means we have trained the neural network model such that, during a fault, when the waveform has an amplitude equal to 1, it means an inter-turn fault occurred in phase ‘a’. Similarly, if the waveform has a value of 2, then the short circuit will be in phase ‘b’ and for an amplitude of 3, the fault will be in phase ‘c’; otherwise, the amplitude will be zero, which means that when there is no fault, the waveform has zero magnitude.

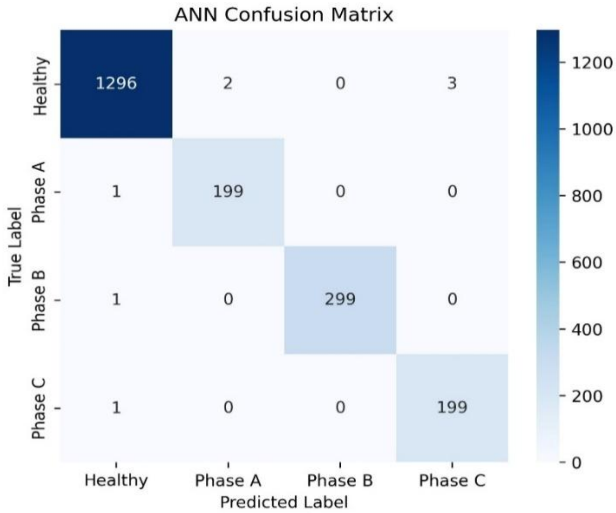


Figure 8. Confusion matrix

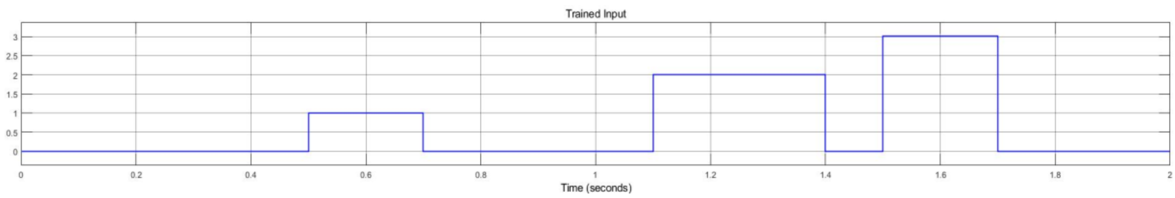


Figure 9. Input provided to the neural network to train the model for identifying a turn fault that occurred in phases a, b, and c

Figure 10(a) shows that, for time 0.5 sec to 0.7 sec, the magnitude of the waveform is nearby or equal to 1, which shows that the fault is in phase ‘a’. Further, for time 1.0 sec to 1.3 sec, the magnitude of the waveform is equal to 2, so it is clear that the short circuit is in phase ‘b’ as shown in Figure 10(b). From time 1.5 sec to 1.7 sec, the magnitude of the waveform is 3, as shown in Figure 10(c), which states that the short circuit is in phase ‘c’. The magnitude of the waveform is ‘zero’ except for these time periods; it means that there is no fault in any phase during the rest of the time. In Figure 10(d), the magnitude is ‘zero’ throughout the duration as there is no fault created in any phase. Which means there is no inter turn fault (ITF) in any phase of stator windings and the system is healthy.

Figure 11(a) shows the statistical characteristics of phase ‘a’ under healthy conditions, whereas Figure 11(b) shows the corresponding characteristics when an ITSC fault is introduced in phase ‘a’. The current magnitude in Figure 11(b) increases to approximately 0.5 p.u., which is about ten times higher than the current ($i_{sa}$) in Figure 11(a), which is approximately 0.05 p.u. A difference in voltage magnitude between Figures 11(a) and 11(b) can also be observed.

Similarly, Figure 11(c) shows the statistical characteristics of phase ‘b’ under healthy conditions, while Figure 11(d) shows the corresponding characteristics when an ITSC fault is introduced in phase ‘b’. As shown in Figure 11(d), the magnitude of the current ($i_{sb}$) increases to approximately 0.7 compared with the healthy condition in Figure 11(c). A change in voltage magnitude can also be observed when the fault is introduced.

Finally, Figure 11(e) presents the statistical characteristics of phase ‘c’ under healthy conditions, whereas Figure 11(f) shows the corresponding characteristics when an ITSC fault is introduced in phase ‘c’. The current ($i_{sc}$) is approximately −0.01 under healthy conditions and increases to approximately 0.07 when the fault occurs in phase ‘c’. A slight difference in voltage magnitude between the healthy and faulty stator winding conditions can also be observed.

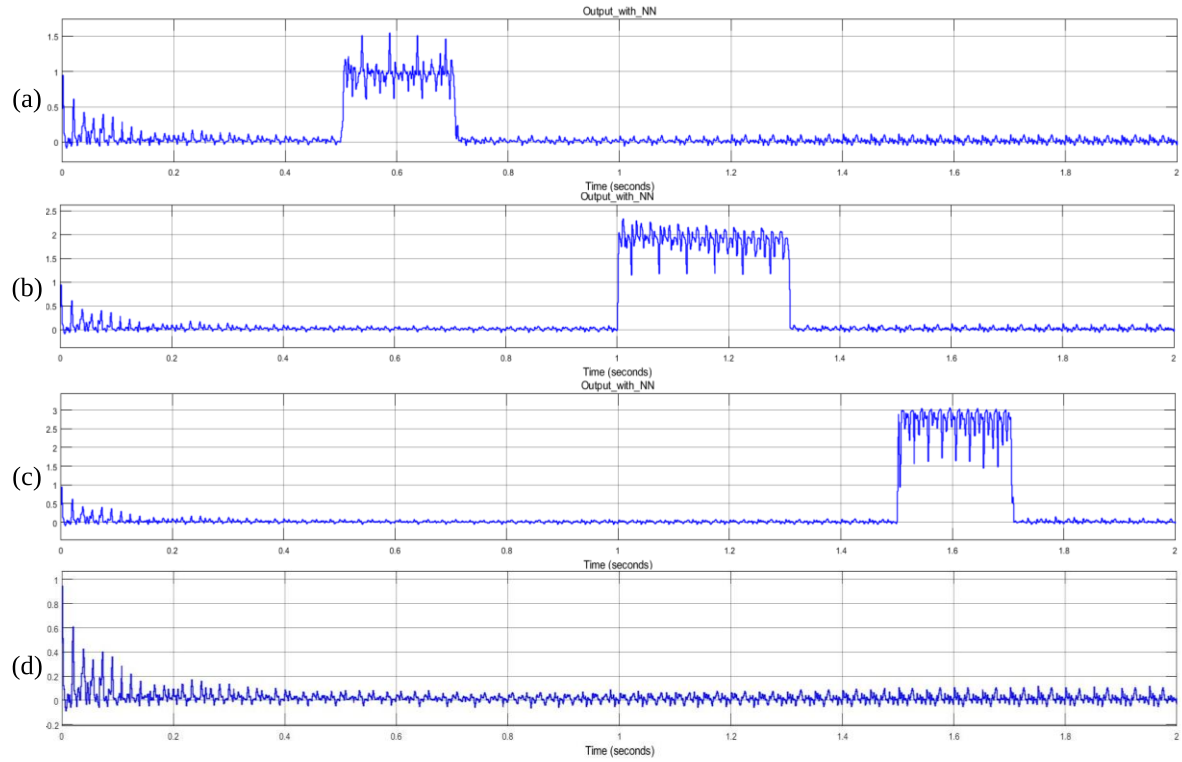


Figure 10. Final output after applying the neural network (NN) in the doubly fed induction generator (DFIG) model: (a) inter-turn fault (ITF) in phase ‘a’ from 0.5 to 0.7 s with an output magnitude of 1, (b) ITF in phase ‘b’ from 1.0 to 1.3 s with an output magnitude of 2, (c) ITF in phase ‘c’ from 1.5 to 1.7 s with an output magnitude of 3, and (d) healthy condition with zero output magnitude throughout the duration

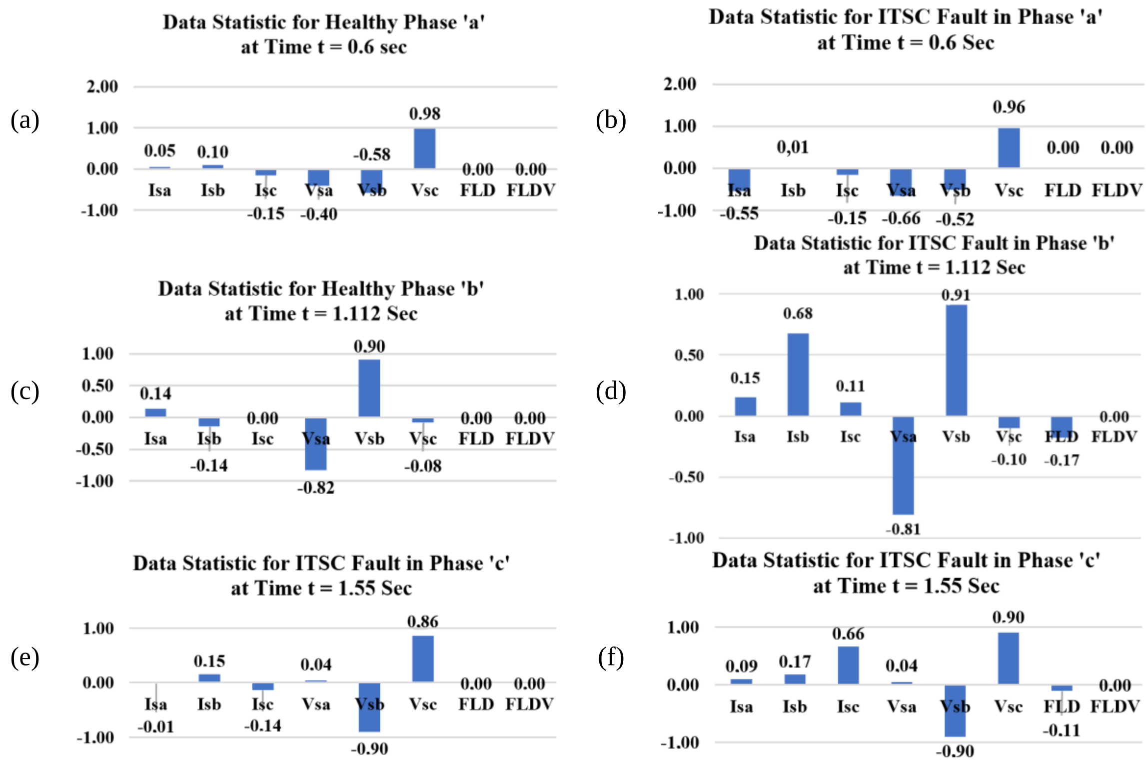


Figure 11. Data statistics of the healthy and faulty DFIG machine for different phases: (a) healthy condition of phase ‘a’, (b) ITSC fault condition in phase ‘a’, (c) healthy condition of phase ‘b’, (d) ITSC fault condition in phase ‘b’, (e) healthy condition of phase ‘c’, and (f) ITSC fault condition in phase ‘c’

## 6. CONCLUSION

The proposed study investigates interturn faults within the stator winding of a DFIG wind turbine. In this context, each phase of the winding in the stator experiences a short circuit, which is characterized by assigning a specific magnitude to each phase. A fault identification method based on FLDV is proposed, employing artificial neural networks to categorize faults at various stages. The accompanying figure depicts the graphical output of the DFIG, including current, voltage, and active & reactive power, under both healthy and faulty conditions. The methodology indicates that the neural network output reflects the amplitude of waveforms 1, 2, or 3 for faults in the respective phases "a," "b," and "c"; otherwise, it records a zero magnitude, signifying the absence of faults when the waveform's magnitude is "0." This approach facilitates early fault detection by analyzing waveform patterns, thereby enabling the prevention of winding overheating due to short circuits and averting severe and permanent damage to the windings. In future applications, IoT-based monitoring, digital twin integration, and multimodal sensing can be implemented to enhance scalability and robustness.

## FUNDING INFORMATION

Authors state no funding involved.

## AUTHOR CONTRIBUTIONS STATEMENT

This journal uses the Contributor Roles Taxonomy (CRediT) to recognize individual author contributions, reduce authorship disputes, and facilitate collaboration.

| Name of Author | C | M | So | Va | Fo | I | R | D | O | E | Vi | Su | P | Fu |
|---|---|---|---|---|---|---|---|---|---|---|---|---|---|---|
| Vivek Kushwaha | ✓ | ✓ | | | ✓ | ✓ | | | ✓ | ✓ | | | | |
| Sanjay Kumar Maurya | ✓ | ✓ | | | | | | | | ✓ | | ✓ | | |
| Arvind Yadav | ✓ | ✓ | | | | | | | | ✓ | | ✓ | | |

C : **C**onceptualization
M : **M**ethodology
So : **So**ftware
Va : **Va**lidation
Fo : **Fo**rmal analysis
I : **I**nvestigation
R : **R**esources
D : **D**ata Curation
O : Writing - **O**riginal Draft
E : Writing - Review & **E**diting
Vi : **Vi**sualization
Su : **Su**pervision
P : **P**roject administration
Fu : **Fu**nding acquisition

## CONFLICT OF INTEREST STATEMENT

Authors state no conflict of interest.

## DATA AVAILABILITY

Data availability is not applicable to this paper as no new data were created or analyzed in this study.

## REFERENCES

[1] H. A. Atteyeh, D. Bayram Kara, A. I. Idriss, and Ş. Serhat Şeker, “Dynamic investigation of a double-fed induction generator under faulty operations,” in *2025 16th International Conference on Electrical and Electronics Engineering (ELECO)*, IEEE, Nov. 2025, pp. 1–5. doi: 10.1109/ELECO69582.2025.11329376.

[2] X. Yin, Y. Shen, Y. Wu, Y. Liu, P. Li, and Q. Ma, “Modeling of stator current signals and drive train fault monitoring applications in doubly-fed induction generator wind turbines,” in *2025 International Conference on Equipment Intelligent Operation and Maintenance (ICEIOM)*, IEEE, Aug. 2025, pp. 668–672. doi: 10.1109/ICEIOM65271.2025.11239543.

[3] H. Liu, Z. Ren, C. Wang, Y. Liu, and X. Wang, “Fault diagnosis of rotor winding short circuit in dfig based on symmetric impedance deviation difference,” in *2025 International Conference on Smart Grid and Sustainable Energy (SGSE)*, IEEE, Jul. 2025, pp. 70–74. doi: 10.1109/SGSE66281.2025.11200314.

[4] M. S. Haider Khan, M. Kumar, and E. S. N. Raju P, “Backstepping control design for DFIG wind turbine system using stator current sensors,” in *2025 IEEE 5th International Conference on Sustainable Energy and Future Electric Transportation (SEFET)*, IEEE, Jul. 2025, pp. 1–6. doi: 10.1109/SEFET65155.2025.11255524.

[5] R. N. Tominaga, R. V. Rocha, S. L. Avila, R. M. Monaro, M. B. de C. Salles, and B. S. Carmo, “DFIG-based wind turbine interturn fault modeling with comprehensive winding failure identification,” *IEEE Transactions on Energy Conversion*, vol. 41, no. 2, pp. 1540–1551, Jun. 2026, doi: 10.1109/TEC.2025.3639143.

[6] C. Gherari, F. Berrezzek, H. Zaimen, and K. Khelil, “Current sensor fault diagnosis of wind power system based on DFIG,” in *2025 International Conference on Artificial Intelligence, Embedded Systems, and Renewable Energy (AIESRE)*, IEEE, Dec. 2025, pp. 1–6. doi: 10.1109/AIESRE67541.2025.11470057.

[7] M. S. Aziz, J. Zhang, S. Ruzimov, L. Sherkhon, and Y. Wu, "Detection of interturn fault in DFIG using zero-sequence voltage component," in *2024 3rd International Conference on Power Systems and Electrical Technology (PSET)*, IEEE, Aug. 2024, pp. 174–180. doi: 10.1109/PSET62496.2024.10808539.

[8] S. Zhao *et al.*, "Fault diagnosis of inter-turn short circuits in doubly-fed induction generators based on external magnetic field and vibration signal fusion," in *2024 International Conference on Sensing, Measurement & Data Analytics in the era of Artificial Intelligence (ICSMD)*, IEEE, Oct. 2024, pp. 1–5. doi: 10.1109/ICSMD64214.2024.10920307.

[9] E. Hamatwi, P. Barendse, and A. Khan, "Evaluating the use of terminal currents and the controller signals in the diagnosis of eccentricity and interturn faults in a micro-DFIG," in *2023 IEEE Energy Conversion Congress and Exposition (ECCE)*, IEEE, Oct. 2023, pp. 4049–4056. doi: 10.1109/ECCE53617.2023.10362125.

[10] S. Zhao *et al.*, "Detecting incipient inter-turn short circuit faults in DFIGs based on magnetic flux leakage theory and MPJ-SVDD analytical method," in *2023 Global Reliability and Prognostics and Health Management Conference (PHM-Hangzhou)*, IEEE, Oct. 2023, pp. 1–8. doi: 10.1109/PHM-Hangzhou58797.2023.10482378.

[11] Y. Chen *et al.*, "Multiscale Park's vector approach for identifying early stator fault severity using MCSA in DFIGs," in *2023 International Conference on Sensing, Measurement & Data Analytics in the era of Artificial Intelligence (ICSMD)*, IEEE, Nov. 2023, pp. 1–4. doi: 10.1109/ICSMD60522.2023.10491041.

[12] B. Battulga, M. F. Shaikh, S. Bin Lee, and M. Osama, "Automated identification of failures in doubly-fed induction generators for wind turbine applications," *IEEE Transactions on Industry Applications*, vol. 59, no. 4, pp. 4454–4463, Jul. 2023, doi: 10.1109/TIA.2023.3257833.

[13] E. Hamatwi, P. Barendse, and A. Khan, "A case for micromachines in laboratory-based DFIG wind turbine systems for fault studies," *IEEE Transactions on Industry Applications*, vol. 59, no. 2, pp. 1754–1764, Mar. 2023, doi: 10.1109/TIA.2022.3232308.

[14] S. Wei, X. Zhang, Y. Xu, Y. Fu, Z. Ren, and F. Li, "Extended Park's vector method in early inter-turn short circuit fault detection for the stator windings of offshore wind doubly-fed induction generators," *IET Generation, Transmission & Distribution*, vol. 14, no. 18, pp. 3905–3912, Sep. 2020, doi: 10.1049/iet-gtd.2020.0127.

[15] A. U. Rehman, Y. Chen, Y. Zhao, Y. Cheng, Y. Zhao, and T. Tanaka, "Detection of rotor inter-turn short circuit fault in doubly-fed induction generator using FEM simulation," in *2018 IEEE 2nd International Conference on Dielectrics (ICD)*, IEEE, Jul. 2018, pp. 1–4. doi: 10.1109/ICD.2018.8468358.

[16] O. Attallah, R. A. Ibrahim, and N. E. Zakzouk, "Fault diagnosis for induction generator-based wind turbine using ensemble deep learning techniques," *Energy Reports*, vol. 8, pp. 12787–12798, Nov. 2022, doi: 10.1016/j.egyr.2022.09.139.

[17] Y. Fu, Z. Ren, S. Wei, Y. Xu, and F. Li, "Using flux linkage difference vector in early inter-turn short circuit detection for the windings of offshore wind DFIGs," *IEEE Transactions on Energy Conversion*, vol. 36, no. 4, pp. 3007–3015, Dec. 2021, doi: 10.1109/TEC.2021.3073007.

[18] Y. Chen *et al.*, "Numerical modeling, electrical characteristics analysis and experimental validation of severe inter-turn short circuit fault conditions on stator winding in DFIG of wind turbines," *IEEE Access*, vol. 9, pp. 13149–13158, 2021, doi: 10.1109/ACCESS.2021.3050876.

[19] K. Ma, J. Zhu, M. Soltani, A. Hajizadeh, and Z. Chen, "Inter-turn short-circuit fault ride-through for DFIG wind turbines," *IFAC-PapersOnLine*, vol. 53, no. 2, pp. 12757–12762, 2020, doi: 10.1016/j.ifacol.2020.12.1916.

[20] F. Bouaziz, O. Awedni, and L. Krichen, "Modelling and fault diagnosis of rotor inter turn short circuit fault in a doubly fed induction generator-based wind turbine," in *2020 20th International Conference on Sciences and Techniques of Automatic Control and Computer Engineering (STA)*, IEEE, Dec. 2020, pp. 189–194. doi: 10.1109/STA50679.2020.9329344.

[21] A. Ur Rehman *et al.*, "Stator inter-turns short circuit fault detection in DFIG using empirical mode decomposition method on leakage flux," in *2020 International Conference on Sensing, Measurement & Data Analytics in the era of Artificial Intelligence (ICSMD)*, IEEE, Oct. 2020, pp. 184–187. doi: 10.1109/ICSMD50554.2020.9261727.

[22] Z. Y. Xue, K. S. Xiahou, M. S. Li, T. Y. Ji, and Q. H. Wu, "Diagnosis of multiple open-circuit switch faults based on long short-term memory network for DFIG-based wind turbine systems," *IEEE Journal of Emerging and Selected Topics in Power Electronics*, vol. 8, no. 3, pp. 2600–2610, Sep. 2020, doi: 10.1109/JESTPE.2019.2908981.

[23] A. U. Rehman *et al.*, "Fault diagnosis in rotor windings in DFIG using magnetic flux measurement coil antenna," in *2019 IEEE Electrical Insulation Conference (EIC)*, IEEE, Jun. 2019, pp. 360–363. doi: 10.1109/EIC43217.2019.9046638.

[24] H. SABIR, M. OUASSAID, and N. NGOTE, "Rotor winding failure diagnosis in wind turbine based on DFIG using the PSD-TSA method," in *2019 8th International Conference on Systems and Control (ICSC)*, IEEE, Oct. 2019, pp. 366–371. doi: 10.1109/ICSC47195.2019.8950520.

[25] I. Idrissi, R. El Bachtiri, H. Chafouk, and M. Khanfara, "Fault diagnosis of stator inter-turn short circuit in doubly fed induction generator of wind turbine," in *2019 6th International Conference on Control, Decision and Information Technologies (CoDIT)*, IEEE, Apr. 2019, pp. 1313–1318. doi: 10.1109/CoDIT.2019.8820697.

[26] T. Sellami, H. Berriri, S. Jelassi, A. M. Darcherif, and M. F. Mimouni, "Performance analysis of grid-connected wind turbine system under Inter-Turn Short-Circuit fault conditions," *International Journal of Renewable Energy Research*, vol. 8, no. 1, pp. 374–383, 2018, doi: 10.20508/ijrer.v8i1.6814.g7312.

[27] H. Sabir, M. Ouassaid, and N. Ngote, "Diagnosis of rotor winding inter-turn short circuit fault in wind turbine based on DFIG using hybrid TSA/DWT approach," in *2018 6th International Renewable and Sustainable Energy Conference (IRSEC)*, IEEE, Dec. 2018, pp. 1–6. doi: 10.1109/IRSEC.2018.8703006.

[28] N. Boumalha, R. Hachelef, D. Kouchih, M. Tadjine, and M. S. Boucherit, "Diagnostic and fault tolerant control by adaptive observer of doubly-fed induction generators with inter-turn rotor and stator fault based wind turbine," in *2017 5th International Conference on Electrical Engineering - Boumerdes (ICEE-B)*, IEEE, Oct. 2017, pp. 1–6. doi: 10.1109/ICEE-B.2017.8192052.

[29] A. Balasubramanian and R. Muthu, "Model based fault detection and diagnosis of doubly fed induction generators – a review," *Energy Procedia*, vol. 117, pp. 935–942, Jun. 2017, doi: 10.1016/j.egypro.2017.05.213.

[30] A. U. Rehman *et al.*, "Experimental research and analysis on rotor winding inter-turn short circuit fault in DFIG," in *2016 International Conference on Condition Monitoring and Diagnosis (CMD)*, IEEE, Sep. 2016, pp. 164–167. doi: 10.1109/CMD.2016.7757776.

[31] A. Ur Rehman, Y. Chen, L. Wang, Y. Zhao, Y. Cheng, and T. Tanaka, "Simulation using MATLAB/Simulink on rotor winding inter-turn short circuit fault in DFIG," in *2016 IEEE International Conference on Dielectrics (ICD)*, IEEE, Jul. 2016, pp. 506–509. doi: 10.1109/ICD.2016.7547653.

[32] L. Wang *et al.*, "Fault diagnosis based on current signature analysis for stator winding of doubly fed induction generator in wind turbine," in *Proceedings of the International Symposium on Electrical Insulating Materials*, IEEE, Jun. 2014, pp. 233–236. doi: 10.1109/ISEIM.2014.6870761.

[33] F. Silva, M. B. Abadi, S. M. A. Cruz, A. P. Gonçalves, A. M. S. Mendes, and A. Ribeiro, "Inter-turn fault detection in doubly-fed induction generators for wind turbine applications using the stator reactive power analysis," in *3rd Renewable Power Generation Conference (RPG 2014)*, Institution of Engineering and Technology, 2014, pp. 8.29-8.29. doi: 10.1049/cp.2014.0914.

[34] L. Jun-qing, W. De-yan, and M. Li, "The research of the inter-turn short circuit of the stator windings in doubly fed induction generator," in *2011 International Conference on Electrical Machines and Systems*, IEEE, Aug. 2011, pp. 1–4. doi: 10.1109/ICEMS.2011.6073603.


## APPENDIX

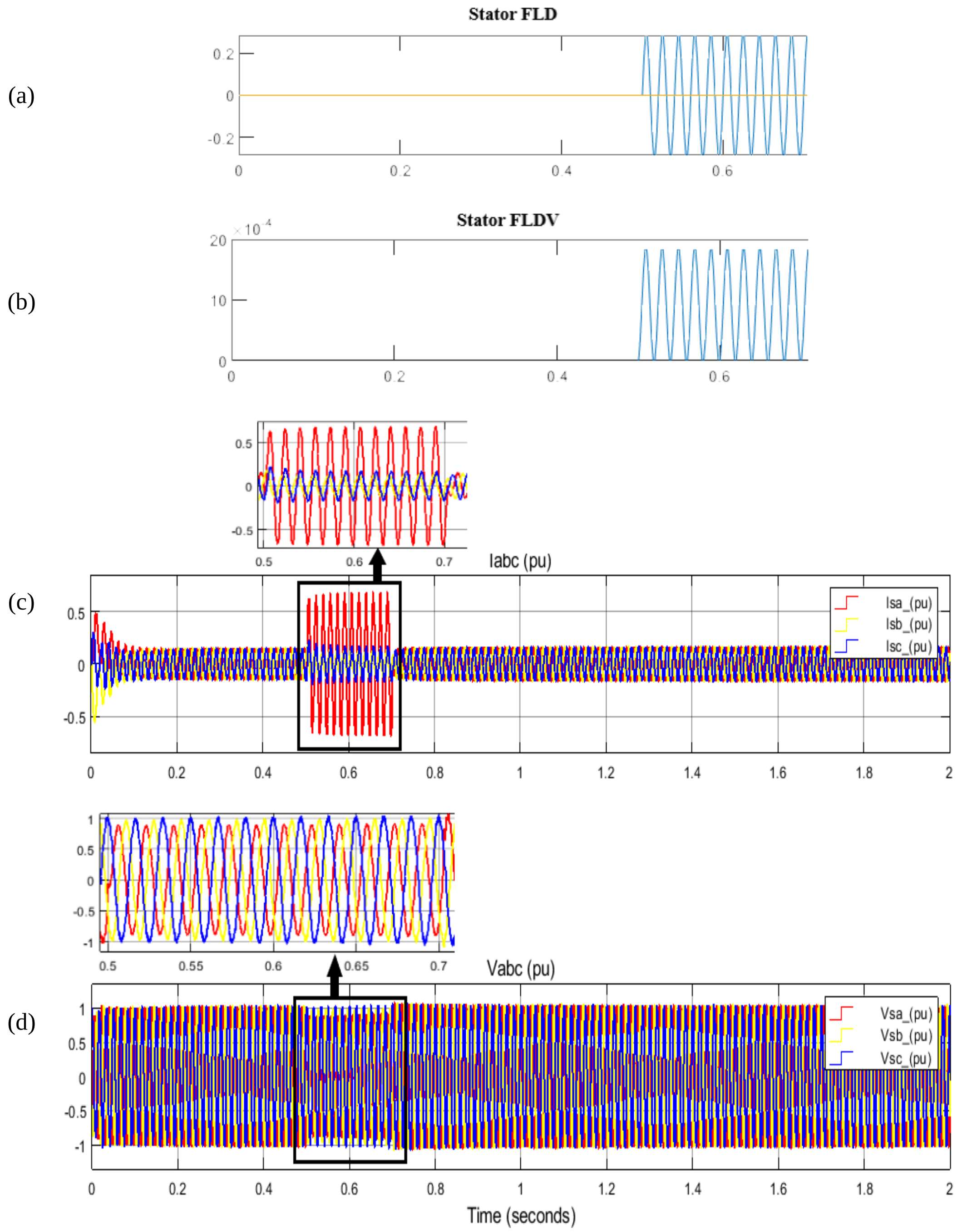


Figure 5. Stator winding responses under inter-turn fault conditions: (a) flux difference (FLD), (b) flux linkage difference vector (FLDV), (c) stator current response for 5 short-circuited turns in phase 'a', and (d) stator voltage response for 5 short-circuited turns in phase 'a'

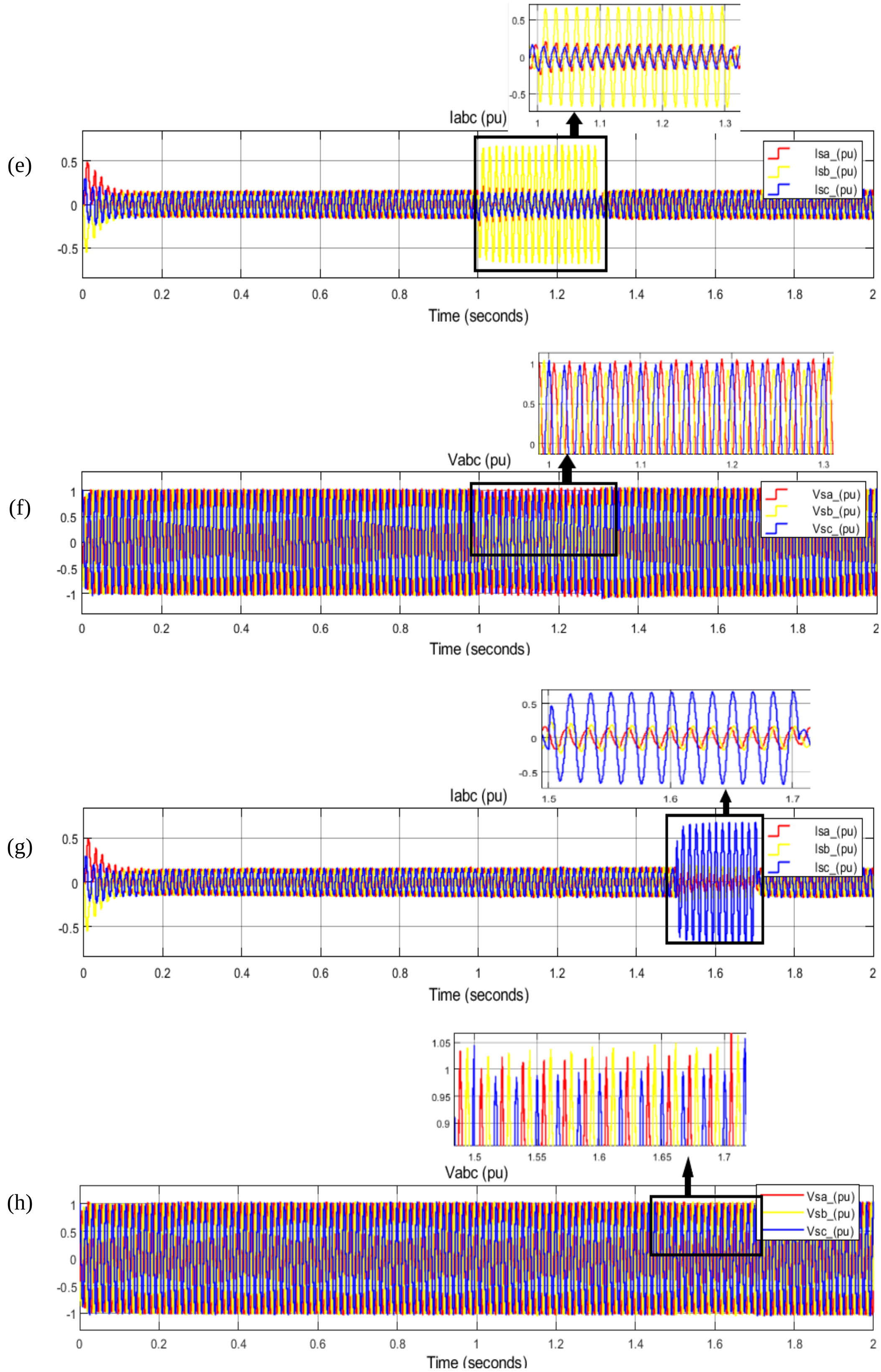


Figure 5. Stator winding responses under inter-turn fault conditions: (e) stator current response for 5 short-circuited turns in phase ‘b’, (f) stator voltage response for 5 short-circuited turns in phase ‘b’, (g) stator current response for 5 short-circuited turns in phase ‘c’, and (h) stator voltage response for 5 short-circuited turns in phase ‘c’

## BIOGRAPHIES OF AUTHORS

**Vivek Kushwaha** received his B.E. degree in Electrical Engineering from Gyan Ganga Institute of Technology and Sciences, Jabalpur, and received his M.E. degree in Control Systems from Jabalpur Engineering College, Jabalpur. His research interests include control systems, grid integration with renewable energy sources, particularly wind turbines, and fault diagnosis in DFIG wind turbines. He is currently an Assistant Professor in the Department of Electrical Engineering at Gyan Ganga Institute of Technology and Sciences, Jabalpur, Madhya Pradesh, India. He is also pursuing a Ph.D. at GLA University, Mathura, Uttar Pradesh, India. He can be contacted at email: vivekkushwaha@ggits.org.

**Sanjay Kumar Maurya** is currently a professor in the Department of Electrical Engineering at Samrat Ashok Rajkiya Engineering College, Mirzapur, Uttar Pradesh, India. Previously, he served as an associate professor in the Department of Electrical Engineering at GLA University, Mathura, India. He received his Ph.D. and M.Tech. degrees from MNNIT Allahabad, Uttar Pradesh, India. He completed his B.Sc. (Engg.) degree in electrical engineering from D.E.I. (Deemed University), Agra, Uttar Pradesh, India. His research interests include multi-stage distribution system planning, hybrid electric vehicles, power electronics, and renewable energy. He can be contacted at email: maurysanjay@gmail.com.

**Arvind Kumar Yadav** received his B.Tech. degree in electrical engineering from Himachal Pradesh University (HPU), India, in 2007, his M.E. degree in power electronics and drives from Punjab Engineering College (PEC), Chandigarh, India, in 2013, and his Ph.D. degree in electrical engineering from GLA University, Mathura, India, in 2021. He has been an associate professor at GLA University. He has authored more than 30 technical papers published in journals, conference proceedings, and book chapters. His research interests include power electronics converters, electric drives, grid integration technologies, applications of power electronics in sustainable renewable energy, and converters for photovoltaic systems. He can be contacted at email: arvind.yadav@gla.ac.in.